Cent. Eur. J. Math. • 11(8) • 2013 • 1478-1488
DOI: 10.2478/s11533-013-0254-4

VERSITA

Central European Journal of **Mathematics**

A parameter-free smoothness indicator for high-resolution finite element schemes

Research Article

Dmitri Kuzmin[1*], Friedhelm Schieweck[2†]

1 *Angewandte Mathematik III, Friedrich-Alexander-Universität Erlangen–Nürnberg, Cauerstr. 11, 91058, Erlangen, Germany*

2 *Institut für Analysis und Numerik, Otto-von-Guericke-Universität Magdeburg, Postfach 4120, 39016, Magdeburg, Germany*

Received 28 February 2012; accepted 11 January 2013

Abstract: This paper presents a postprocessing technique for estimating the local regularity of numerical solutions in high-resolution finite element schemes. A derivative of degree $p \geq 0$ is considered to be smooth if a discontinuous linear reconstruction does not create new maxima or minima. The intended use of this criterion is the identification of smooth cells in the context of p-adaptation or selective flux limiting. As a model problem, we consider a 2D convection equation discretized with bilinear finite elements. The discrete maximum principle is enforced using a linearized flux-corrected transport algorithm. The deactivation of the flux limiter in regions of high regularity makes it possible to avoid the peak clipping effect at smooth extrema without generating spurious undershoots or overshoots elsewhere.

MSC: 65N30

Keywords: Finite elements • Maximum principles • Smoothness indicators • Gradient recovery • Slope limiting • Flux-corrected transport • p-adaptation

1. Introduction

The design of high-resolution finite element schemes for convection-dominated transport problems requires certain modifications of the standard Galerkin approximation in regions where unresolved small-scale features are present. To prevent nonphysical oscillations in these regions, the numerical scheme must contain a mechanism for adaptively reducing the order of approximation and/or generating shock-capturing artificial diffusion. In discontinuous Galerkin

* *E-mail: kuzmin@am.uni-erlangen.de*
† *E-mail: schiewec@ovgu.de*

(DG) methods, this task is commonly accomplished by means of slope limiters that switch to a piecewise-constant approximation in "troubled" cells [1, 2, 4, 6, 11, 16]. Obviously, this approach is not an option in the context of continuous finite element schemes. The discrete maximum principle for (bi-)linear approximations can be enforced, e.g., using the flux-corrected transport (FCT) algorithm [3, 5]. However, its extension to higher-order finite elements is still an open problem.

The use of limiting techniques increases the computational cost and may degrade the order of accuracy at smooth extrema. On the other hand, it is generally safe to use the standard Galerkin method and higher-order basis functions in elements where the numerical solution exhibits sufficient regularity. For this reason, many strategies for identifying "smooth" and "troubled" cells have been proposed in the literature [2, 4, 11–13, 16]. A typical troubled cell marker for DG methods measures the interelement jumps or highest-order components of the shape function. A smoothness indicator for deactivation of shock capturing terms in continuous stabilized finite element schemes was designed in [15] using a simple postprocessing technique. The difference between the numerical solution and its reconstruction from cell averages was found to be a good shock detector.

It is relatively easy to design a sensor that has large values in the neighborhood of discontinuities and small values in smooth regions. However, there is no simple way to find the threshold for a troubled cell marker. The use of fixed tolerances for the absolute or relative values of smoothness sensors may result in a poor estimate of local regularity [11]. The failure to detect a trouble cell may cause a violation of the maximum principle and give rise to numerical instabilities. Another alarming side effect is the loss of accuracy due to unnecessary limiting in unrecognized smooth cells. Last but not least, heuristic indicators are unable to predict if the local regularity is sufficient for p-enrichment to be safe and profitable.

In this paper, we introduce a hierarchical smoothness estimator for the solution and its partial derivatives. It is somewhat similar to the postprocessing indicator employed in [15] but the reconstructed solution is generally discontinuous, and no free parameters are involved. The proposed approach to regularity analysis is based on the same design philosophy as the hierarchical vertex-based slope limiter developed by the first author for DG approximations to hyperbolic conservation laws [6, 7]. When it comes to regularity estimation for a derivative of degree $p \geq 0$, we use variational gradient recovery to compute the $(p+1)$-st derivatives and define a discontinuous reconstruction in each cell. The p-th derivative is smooth if the reconstructed shape function is bounded by the original values at cell centers. No flux limiting is required if a smooth derivative is found. If the highest-order derivative is smooth, then the cell is a candidate for p-enrichment. To assess the usefulness of the new smoothness sensor, we use it to activate and deactivate the flux limiter in an FEM-FCT discretization of a linear convection equation. The first results indicate that the proposed methodology is well suited for this purpose.

2. Regularity estimator

We begin with the presentation of the postprocessing technique for estimating the local regularity of continuous (multi-)linear finite element approximations. Its extension to higher-order elements and DG methods is straightforward.

Let $u_h \in V_h$ denote a finite element approximation to the weak solution $u \in V$ of a given (initial–)boundary value problem. Since we are interested in estimating the regularity of u_h, our analysis will be independent of the underlying PDE. The restriction of u_h to a single element K of the computational mesh $\mathcal{T}_h$ is given by a linear or bilinear shape function $u_h|_K$. To estimate the smoothness of u_h in a neighborhood of cell K, we consider a linear approximation of the form

$$\widehat{u}_h(\mathbf{x}) = u_h(\mathbf{x}_c) + R_h u_h(\mathbf{x}_c) \cdot (\mathbf{x} - \mathbf{x}_c), \tag{1}$$

where $\mathbf{x}_c$ denotes the center of K and $R_h \colon V_h \to V_h \times V_h$ is a gradient recovery operator. In contrast to ∇u_h, the reconstructed gradient is continuous, and $R_h u_h(\mathbf{x}_c)$ depends on the data in all elements that share a vertex with K. In this paper, we construct $R_h u_h = (R_h^1 u_h, R_h^2 u_h)^T$ using an L^2 projection (see the next section).

The shape functions given by (1) define a **discontinuous** piecewise-linear approximation $\widehat{u}_h$. The difference between u_h and $\widehat{u}_h$ may serve as a smoothness indicator. We label the cell K as smooth if the value of $\widehat{u}_h$ at each vertex $\mathbf{x}_i \in K$ is bounded by the values of u_h at the centers of surrounding elements thus

$$u_i^{\min} < \widehat{u}_h(\mathbf{x}_i) < u_i^{\max} \qquad \text{for all} \quad \mathbf{x}_i \in K, \tag{2}$$

where

$$\begin{aligned} u_i^{\max} &= \max\big\{u_h(\mathbf{x}_c) : \text{there exists } K \in \mathcal{T}_h \text{ such that } \mathbf{x}_i, \mathbf{x}_c \in K\big\}, \\ u_i^{\min} &= \min\big\{u_h(\mathbf{x}_c) : \text{there exists } K \in \mathcal{T}_h \text{ such that } \mathbf{x}_i, \mathbf{x}_c \in K\big\}. \end{aligned} \tag{3}$$

In DG methods, such maximum principles can be enforced by limiting the derivatives of $\widehat{u}_h$. Hence, the proposed regularity criterion is equivalent to the application of a vertex-based slope limiter [6, 7] to the postprocessed solution $\widehat{u}_h$. Note that the inequalities in (2) are strict, which implies that a constant function is not regarded as smooth. This convention is adopted to avoid unnecessary p-refinements in the context of hp-adaptivity. In practice, we use inequality constraints of the form $u_i^{\min} + \epsilon < \widehat{u}_h(\mathbf{x}_i) < u_i^{\max} - \epsilon$, where ϵ is a small positive number.

Since conditions (2)–(3) are violated at the local maxima and minima of u_h, all cells containing these extrema are marked as "troubled" [11]. To distinguish between smooth peaks and spurious undershoots/overshoots, the regularity estimator must be applied to each component of the gradient $\nabla u_h = (u_x, u_y)^{\mathsf{T}}$.

Building on the analogy with [6, 7], we use the derivatives of the recovered gradient $R_h u_h = (R_h^1 u_h, R_h^2 u_h)^{\mathsf{T}}$ to define the linear reconstructions

$$\widehat{u}_h^1(\mathbf{x}) = \frac{\partial u_h}{\partial x}(\mathbf{x}_c) + \nabla R_h^1 u_h(\mathbf{x}_c) \cdot (\mathbf{x} - \mathbf{x}_c), \qquad \widehat{u}_h^2(\mathbf{x}) = \frac{\partial u_h}{\partial y}(\mathbf{x}_c) + \nabla R_h^2 u_h(\mathbf{x}_c) \cdot (\mathbf{x} - \mathbf{x}_c). \tag{4}$$

The gradient is regarded as smooth if the values of $\widehat{u}_h^1$ and $\widehat{u}_h^2$ at all vertices of K are bounded by the centroid values of $\partial u_h/\partial x$ and $\partial u_h/\partial y$, respectively. The corresponding maximum principle is given by (2)–(3) with $\widehat{u}_h$ replaced by $\widehat{u}_h^k$, $k = 1, 2$.

As shown in [6, 7], no shock capturing is required if the finite element solution u_h and/or both components of its gradient are found to be smooth. Since the regularity estimates for the derivatives w.r.t. x and y are independent, they may be used to steer anisotropic refinement in hp-adaptive finite element codes.

3. Gradient reconstruction

Many a posteriori error estimates for adaptive finite element schemes are based on gradient recovery techniques [18]. Given a finite element solution $u_h \in V_h$, where $V_h = \operatorname{span}\{\varphi_1, \ldots, \varphi_N\}$, the operator $R_h : V_h \to V_h \times V_h$ is defined by

$$R_h^k u_h = \sum_{j=1}^{N} g_j^k \varphi_j, \qquad k = 1, 2. \tag{5}$$

The coefficients $g_j^1 \approx (\partial u/\partial x)(\mathbf{x}_j)$ and $g_j^2 \approx (\partial u/\partial y)(\mathbf{x}_j)$ can be determined, e.g., using superconvergent patch recovery [19, 20] or the general transfer operator developed by the second author [14]. Another popular recovery technique is the L^2 projection

$$\int_\Omega \varphi_i R_h u_h \, \mathrm{d}\mathbf{x} = \int_\Omega \varphi_i \nabla u_h \, \mathrm{d}\mathbf{x}, \qquad i = 1, \ldots, N.$$

Invoking (5), one obtains the linear systems for the vectors of nodal derivatives

$$M_C g^k = b^k, \tag{6}$$

where $M_C = \{m_{ij}\}$ is the consistent mass matrix and $b^k = \{b_i^k\}$, $k = 1, 2$, is the load vector associated with the k-th derivative. By virtue of (6), we have

$$m_{ij} = \int_\Omega \varphi_i \varphi_j \, \mathrm{d}\mathbf{x}, \qquad (b_i^1, b_i^2)^{\mathsf{T}} = \int_\Omega \varphi_i \nabla u_h \, \mathrm{d}\mathbf{x}.$$

Since the mass matrix M_C is well-conditioned, the cost of solving a linear system of the form (6) is rather low. We remark that the use of row-sum mass lumping would produce a smooth low-order approximation to ∇u. As a result, the smoothness sensor based on (1) and (4) may overestimate the local regularity. For this reason, it is essential to use the consistent-mass version of the L^2 projection.

4. Algebraic flux correction

We will estimate the regularity of finite element approximations to the weak solution of the unsteady linear convection equation

$$\frac{\partial u}{\partial t} + \nabla \cdot (\mathbf{v} u) = 0 \qquad \text{in} \quad \Omega, \tag{7}$$

where u is the concentration of a conserved quantity, $\mathbf{v}$ is a given velocity field, and Ω is a bounded domain. Since equation (7) is of hyperbolic type, we prescribe a Dirichlet boundary condition on the inflow part of the boundary Γ,

$$u = u_D \qquad \text{on} \quad \Gamma_D = \{\mathbf{x} \in \Gamma : \mathbf{v} \cdot \mathbf{n} < 0\},$$

where $\mathbf{n}$ is the unit outward normal to Γ. The initial condition is given by $u(\mathbf{x}, 0) = u_0(\mathbf{x})$, $\mathbf{x} \in \Omega$. The discretization in space by the standard or stabilized Galerkin method yields a system of equations that can be written in the generic form

$$M_C \frac{du}{dt} = Ku, \tag{8}$$

where u is the vector of time-dependent nodal values, $M_C = \{m_{ij}\}$ is the consistent mass matrix, and $K = \{k_{ij}\}$ is the discrete transport operator.

A semi-discrete scheme of the form (8) proves *local extremum diminishing* (for $\nabla \cdot \mathbf{v} = 0$ only) and positivity-preserving (for any $\mathbf{v}$) if $m_{ii} > 0$, $m_{ij} = 0$, $k_{ij} \geq 0$ for all $j \neq i$; see [8, 9]. The standard Galerkin discretization fails to satisfy these sufficient conditions and gives rise to nonphysical oscillations in "troubled" cells. To enforce the maximum principle in these cells, we will use algebraic flux correction [8] to control the contribution of matrix entries that have a wrong sign ($m_{ij} > 0$ and $k_{ij} < 0$).

To begin with, we replace the matrix M_C with its lumped counterpart

$$M_L = \operatorname{diag}\{m_i\}, \qquad m_i = \sum_j m_{ij}.$$

Next, we fix K by adding a discrete diffusion operator $D = \{d_{ij}\}$ with $d_{ij} = \max\{-k_{ij}, 0, -k_{ji}\} = d_{ji}$ for $j \neq i$ [8, 9], so that $K + D$ has no negative off-diagonal coefficients. The diagonal entries of D are defined so that this symmetric matrix has zero row sums $d_{ii} = -\sum_{j \neq i} d_{ij}$. Due to symmetry, the column sums are also equal to zero. In the 1D case, the lumped-mass Galerkin approximation on a uniform mesh of linear finite elements is equivalent to the central difference scheme, while the modified operator $K + D$ corresponds to the first-order upwind difference [9].

In summary, the semi-discrete Galerkin scheme (8) can be split as follows:

$$M_L \frac{du}{dt} = (K + D)u + f(u),$$

where $f(u)$ is the sum of antidiffusive terms that may destroy positivity

$$f(u) = (M_L - M_C)\frac{du}{dt} - Du. \tag{9}$$

Since $M_L - M_C$ and D are symmetric with zero row sums, we have

$$\begin{aligned}(M_L u - M_C u)_i &= m_i u_i - \sum_j m_{ij} u_j = \sum_{j\neq i} m_{ij}(u_i - u_j),\\ (Du)_i &= \sum_j d_{ij} u_j = d_{ii} u_i + \sum_{j\neq i} d_{ij} u_j = \sum_{j\neq i} d_{ij}(u_j - u_i).\end{aligned} \tag{10}$$

Thus, each component of (9) admits a flux decomposition of the form $f_i = \sum_{j\neq i} f_{ij}$, $f_{ji} = -f_{ij}$. The formula for the *raw antidiffusive fluxes* f_{ij} follows from (10),

$$f_{ij} = \left(m_{ij}\frac{\mathrm{d}}{\mathrm{d}t} + d_{ij}\right)(u_i - u_j), \qquad j \neq i.$$

Some fluxes are harmless but others may create undershoots or overshoots in proximity to troubled cells. The contribution of these "bad" fluxes must be limited so as to make the antidiffusive term local extremum diminishing. After this correction, the generic form of the semi-discrete problem becomes

$$M_L \frac{\mathrm{d}u}{\mathrm{d}t} = (K + D)u + \bar{f}(u), \tag{11}$$

where $\bar{f}(u)$ is a vector containing the sums of limited antidiffusive fluxes

$$\bar{f}_i = \sum_{j\neq i} \alpha_{ij} f_{ij}, \qquad 0 \leq \alpha_{ij} \leq 1.$$

A well-designed flux limiter produces $\alpha_{ij} \approx 1$ in smooth regions and $\alpha_{ij} = 0$ in troubled cells. We will calculate the correction factors using a nonclipping version of Zalesak's limiter [17] presented in the next section.

In the numerical examples that follow, we discretize (11) in time using the Crank–Nicolson method. The result is a nonlinear algebraic system

$$Au^{n+1} = Bu^n + \bar{f}, \tag{12}$$

where $\bar{f}$ is the fully discrete counterpart of the limited antidiffusive term,

$$\begin{aligned}A &= \frac{1}{\Delta t} M_L - \frac{1}{2}(K + D),\\ B &= \frac{1}{\Delta t} M_L + \frac{1}{2}(K + D).\end{aligned} \tag{13}$$

Since the implicit part of $\bar{f}$ depends on the unknown solution u^{n+1}, it must be linearized or calculated in an iterative way. We will use an FCT algorithm [5, 9] in which the raw antidiffusive fluxes

$$f_{ij} = \left(\frac{m_{ij}}{\Delta t} + \frac{d_{ij}}{2}\right)(u_i^* - u_j^*) - \left(\frac{m_{ij}}{\Delta t} - \frac{d_{ij}}{2}\right)(u_i^n - u_j^n)$$

are evaluated using the unconstrained Galerkin approximation u^* to $u(t^{n+1})$.

5. Limiting strategy

In this section, we present Zalesak's limiter [17] that we use to calculate the correction factors α_{ij}. The right-hand side of (12) is a vector with components

$$b_i = \frac{m_i}{\Delta t}\widetilde{u}_i + \sum_{j\neq i}\alpha_{ij}f_{ij}, \tag{14}$$

where $\widetilde{u} = M_L^{-1}\Delta t B u^n$ is an explicit low-order approximation to $u(t^{n+1/2})$. As shown in [8, 9], it inherits positivity of u^n under the CFL-like condition

$$\Delta t \leq -\frac{2m_i}{k_{ii}+d_{ii}} \qquad \text{for all} \quad i.$$

Let $S_i = \{j \neq i : m_{ij} \neq 0\}$ be the set of nearest neighbors of node i. The local maxima and minima of the auxiliary solution $\widetilde{u}$ are given by

$$u_i^{\max} = \max\left\{\widetilde{u}_i, \max_{j\in S_i}\widetilde{u}_j\right\}, \qquad u_i^{\min} = \min\left\{\widetilde{u}_i, \min_{j\in S_i}\widetilde{u}_j\right\}.$$

In accordance with the FCT philosophy, the flux limiting procedure must render the antidiffusive term local extremum diminishing. To this end, the constrained solution to (14) must satisfy the local discrete maximum principle

$$m_i u_i^{\min} \leq \Delta t b_i \leq m_i u_i^{\max}. \tag{15}$$

The process of flux correction begins with the optional "prelimiting" step

$$f_{ij} \overset{\text{def}}{=} 0 \qquad \text{if} \quad f_{ij}(\widetilde{u}_j - \widetilde{u}_i) > 0.$$

This adjustment was found to eliminate spurious ripples created by fluxes that flatten the solution profiles instead of steepening them [8, 17].

The choice of the correction factors α_{ij} must guarantee that a positive sum of limited antidiffusive fluxes $\alpha_{ij}f_{ij}$ cannot create an overshoot, and its negative counterpart cannot create an undershoot. Assuming the worst-case scenario, we enforce condition (15) using Zalesak's multidimensional FCT algorithm [17]:

1. Compute the sums of positive and negative antidiffusive fluxes

$$P_i^+ = \sum_{j\neq i}\max\{0, f_{ij}\}, \qquad P_i^- = \sum_{j\neq i}\min\{0, f_{ij}\}.$$

2. Define the upper and lower bounds for admissible increments

$$Q_i^+ = \frac{m_i}{\Delta t}(u_i^{\max} - \widetilde{u}_i), \qquad Q_i^- = \frac{m_i}{\Delta t}(u_i^{\min} - \widetilde{u}_i).$$

3. Compute the nodal correction factors for the components of $P_i^{\pm}$

$$R_i^+ = \min\left\{1, \frac{Q_i^+}{P_i^+}\right\}, \qquad R_i^- = \min\left\{1, \frac{Q_i^-}{P_i^-}\right\}.$$

4. Check the sign of the unconstrained flux and multiply f_{ij} by

$$\alpha_{ij} = \begin{cases} \min\{R_i^+, R_j^-\} & \text{if} \quad f_{ij} > 0, \\ \min\{R_i^-, R_j^+\} & \text{if} \quad f_{ij} < 0. \end{cases}$$

This symmetric limiting strategy guarantees that (15) holds for both nodes. By the M-matrix property of (13), positivity of $\widetilde{u}$ carries over to u^{n+1} [8, 9].

A disturbing side effect associated with flux correction of FCT type is known as *clipping* [8, 17]. Since the sum of limited antidiffusive fluxes is forced to be local extremum diminishing, even smooth peaks lose a little bit of amplitude after each time step. To avoid peak clipping, we deactivate the flux limiter by setting

$$R_i^{\pm} = 1$$

at vertices surrounded by smooth cells. These vertices are identified using the regularity estimate for the *gradient* of the auxiliary solution $\widetilde{u}$. Since the solution has higher regularity than its derivatives, it is also safe to deactivate the limiter in cells where conditions (2)–(3) hold for the linear reconstruction given by (1).

6. Numerical results

To illustrate the capability of the hierarchical regularity estimator to locate shocks and smooth peaks, we perform a numerical study for the *solid body rotation* problem [3, 10]. In this example, we solve equation (7) with the velocity field

$$\mathbf{v}(x, y) = (0.5 - y, x - 0.5)$$

which describes a counterclockwise rotation about the center of $\Omega = (0, 1) \times (0, 1)$.

The exact solution to the solid body rotation problem reproduces the initial state u_0 exactly after each full revolution ($t = 2\pi k$, $k \in \mathbb{N}$). Hence, the challenge of this test is to preserve the shape of u_0. Following LeVeque [10], we consider a slotted cylinder, a sharp cone, and a smooth hump, see Figure 1. Initially, the geometry of each body is given by a function $G(x, y)$ defined within the circle

$$r(x, y) = \frac{1}{r_0}\sqrt{(x - x_0)^2 + (y - y_0)^2} \leq 1$$

of radius $r_0 = 0.15$ centered at a point with Cartesian coordinates (x_0, y_0).

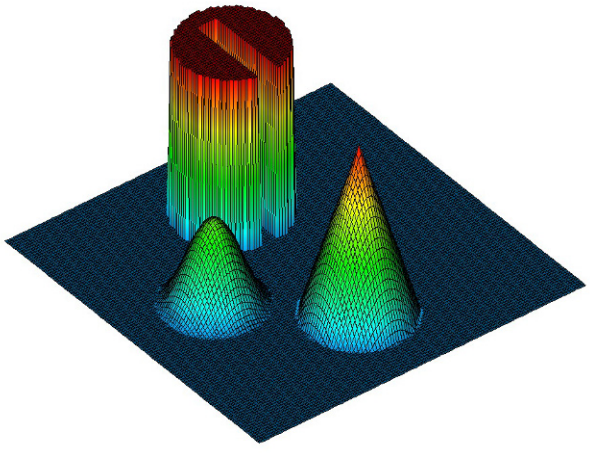

Figure 1. Initial data / exact solution at the final time $t = 2\pi$.

For the slotted cylinder, the reference point is $(x_0, y_0) = (0.5, 0.75)$ and [10]

$$G(x,y) = \begin{cases} 1 & \text{if} \quad |x - x_0| \geq 0.025 \quad \text{or} \quad y \geq 0.85, \\ 0 & \text{otherwise.} \end{cases}$$

The cone is centered at $(x_0, y_0) = (0.5, 0.25)$ and its geometry is defined by

$$G(x,y) = 1 - r(x,y).$$

The peak of the hump is located at $(x_0, y_0) = (0.25, 0.5)$ and the shape is

$$G(x,y) = \frac{1 + \cos(\pi r(x,y))}{4}.$$

The diagrams in Figure 2 show the results of regularity estimation for the above initial data projected onto a uniform mesh of 128×128 bilinear elements. The smoothness sensor η_i^0 equals 1 if conditions (2)–(3) hold in all elements containing the vertex $\mathbf{x}_i$. If this is not the case, we set $\eta_i^0 = 0$. The markers η_i^1 and η_i^2 measure the regularity of the derivatives w.r.t. x and y. The last marker is defined as $\eta_i^{\max} = \max\{\eta_i^0, \min\{\eta_i^1, \eta_i^2\}\}$. In Figure 2, the marker values 0 and 1 are shown in blue and red, respectively. In accordance with criterion (2), all nodes inside or around the slotted cylinder are marked as non-smooth since the solution is piecewise-constant in this region. The deactivation of flux limiting at vertices with $\eta_i^1 = \eta_i^2 = 1$ or $\eta_i^{\max} = 1$ makes it possible to avoid peak clipping without generating undershoots or overshoots in the neighborhood of discontinuities.

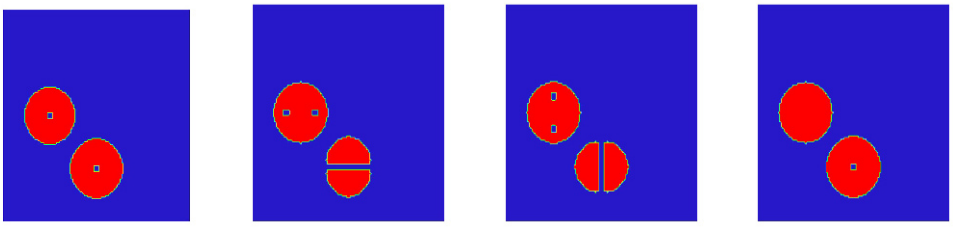

(a) η^0 (b) η^1 (c) η^2 (d) $\eta^{\max}$

Figure 2. Solid body rotation: regularity of the initial data.

The numerical solutions displayed in Figure 3 were obtained with the global and local versions of the FCT limiter using the Crank–Nicolson time-stepping and $\Delta t = 10^{-3}$. For a better comparison, the solution profiles along the lines $y = 0.5$ and $x = 0.5$ are presented in Figures 4 and 5, respectively. It can readily be seen that the local version of the FCT limiter yields a much better resolution of the smooth hump and a minor reduction in peak clipping at the tip of the cone. The results for the slotted cylinder are identical since all nodes located in proximity to discontinuities are correctly identified as non-smooth. We remark that the small local maximum at $x \approx 0.625$ is caused by numerical diffusion that gradually increases the values of u in the middle of the slot. In summary, the recovery-based smoothness sensor yields a quite realistic estimate of local regularity. The numerical cost of recovery-based regularity estimation is comparable to that of global flux limiting. This added cost may be compensated by skipping the smooth nodes when it comes to computation of nodal correction factors for the FCT.

As shown by John and Schmeyer [3], the solid body rotation problem is a challenging test for stabilized finite element methods. Therefore, we feel that the results presented in this section are representative enough to draw preliminary conclusions regarding the quality of local regularity estimates. Of course, there is no guarantee that the new marker will perform so well for all problems of practical interest. For example, it might fail to recognize a discontinuity smeared by numerical diffusion. This problem can be cured using adaptive mesh refinement.

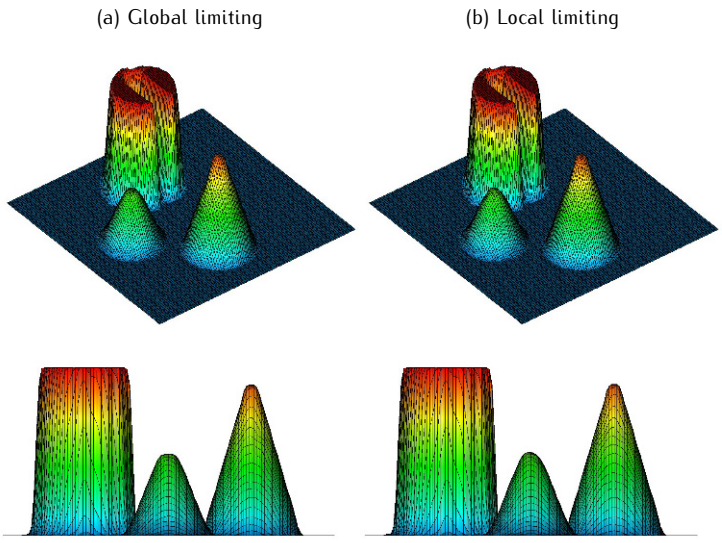

Figure 3. Solid body rotation: FEM-FCT solutions at $t = 2\pi$.

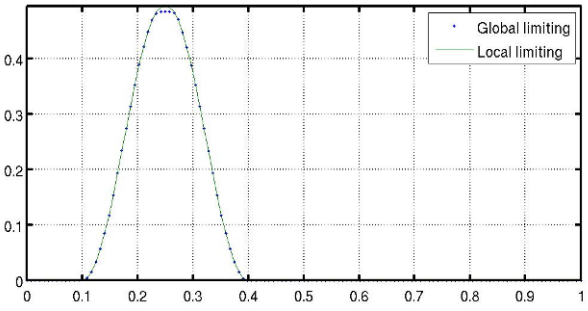

Figure 4. Solid body rotation: FEM-FCT solution profiles at $y = 0.5$.

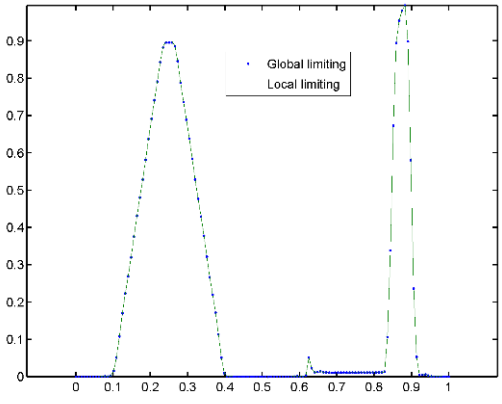

Figure 5. Solid body rotation: FEM-FCT solution profiles at $x = 0.5$.

7. Conclusions

This note sheds some light on various aspects of a posteriori regularity estimation for adaptive high-resolution finite element schemes. We have shown that the variations of derivatives play an important role in the detection of smooth cells. Hierarchical smoothness sensors based on variational gradient recovery provide a useful tool for the design of troubled cell markers and adaptive p-refinement strategies for continuous and discontinuous finite elements. The lack of free parameters makes the proposed methodology an attractive alternative to traditional smoothness sensors. In particular, we envisage its usage in the context of hp-adaptive finite element schemes for convection-dominated transport problems.

Acknowledgements

The authors would like to thank Melanie Bittl (Friedrich-Alexander-Universität Erlangen–Nürnberg) and Dr. Piotr Skrzypacz (Otto-von-Guericke Universität Magdeburg) for inspiring discussions. This research was supported by the German Research Association (DFG) under grant KU 1530/6-1.

References

[1] Cockburn B., Shu C.-W., The Runge–Kutta discontinuous Galerkin method for conservation laws V: Multidimensional systems, J. Comput. Phys., 1998, 141(2), 199–224

[2] Dolejší V., Feistauer M., On the discontinuous Galerkin method for the numerical solution of compressible high-speed flow, In: Numerical Mathematics and Advanced Applications, Ischia, July, 2001, Springer, Milan, 2003, 65–83

[3] John V., Schmeyer E., On finite element methods for time-dependent convection-diffusion-reaction equations with small diffusion, Comput. Methods Appl. Mech. Engrg., 2008, 198(3-4), 475–494

[4] Krivodonova L., Xin J., Remacle J.-F., Chevaugeon N., Flaherty J.E., Shock detection and limiting with discontinuous Galerkin methods for hyperbolic conservation laws, In: Workshop on Innovative Time Integrators for PDEs, Appl. Numer. Math., 2004, 48(3-4), 323–338

[5] Kuzmin D., Explicit and implicit FEM-FCT algorithms with flux linearization, J. Comput. Phys., 2009, 228(7), 2517–2534

[6] Kuzmin D., A vertex-based hierarchical slope limiter for p-adaptive discontinuous Galerkin methods, J. Comput. Appl. Math., 2010, 233(12), 3077–3085

[7] Kuzmin D., Slope limiting for discontinuous Galerkin approximations with a possibly non-orthogonal Taylor basis, Internat. J. Numer. Methods Fluids, 2013, 71(9), 1178–1190

[8] Kuzmin D., Möller M., Algebraic flux correction I. Scalar conservation laws, In: Flux-Corrected Transport, Sci. Comput., Springer, Berlin, 2005, 155–206

[9] Kuzmin D., Turek S., Flux correction tools for finite elements, J. Comput. Phys., 2002, 175(2), 525–558

[10] LeVeque R.J., High-resolution conservative algorithms for advection in incompressible flow, SIAM J. Numer. Anal., 1996, 33(2), 627–665

[11] Michoski C., Mirabito C., Dawson C., Wirasaet D., Kubatko E.J., Westerink J.J., Adaptive hierarchic transformations for dynamically p-enriched slope-limiting over discontinuous Galerkin systems of generalized equations, J. Comput. Phys., 2010, 230(22), 8028–8056

[12] Persson P.-O., Peraire J., Sub-cell shock capturing for discontinuous Galerkin methods, In: 44th AIAA Aerospace Sciences Meeting, Reno, January, 2006, preprint available at http://acdl.mit.edu/peraire/PerssonPeraire_ShockCapturing.pdf

[13] Qiu J., Shu C.-W., A comparison of troubled-cell indicators for Runge–Kutta discontinuous Galerkin methods using weighted essentially nonoscillatory limiters, SIAM J. Sci. Comput. 2005, 27(3), 995–1013

[14] Schieweck F., A general transfer operator for arbitrary finite element spaces, Preprint 25/00, Otto-von-Guericke Universität Magdeburg, 2000

[15] Schieweck F., Skrzypacz P., A local projection stabilization method with shock capturing and diagonal mass matrix for solving non-stationary transport dominated problems, Comput. Methods Appl. Math., 2012, 12(2), 221–240
[16] Yang M., Wang Z.J., A parameter-free generalized moment limiter for high-order methods on unstructured grids, Adv. Appl. Math. Mech., 2009, 1(4), 451–480
[17] Zalesak S.T., Fully multidimensional flux-corrected transport algorithms for fluids, J. Comput. Phys., 1979, 31(3), 335–362
[18] Zienkiewicz O.C., Zhu J.Z., A simple error estimator and adaptive procedure for practical engineering analysis, Internat. J. Numer. Methods Engrg., 1987, 24(2), 337–357
[19] Zienkiewicz O.C., Zhu J.Z., The superconvergent patch recovery and a posteriori error estimates. Part 1: The recovery technique, Internat. J. Numer. Methods Engrg., 1992, 33(7), 1331–1364
[20] Zienkiewicz O.C., Zhu J.Z., The superconvergent patch recovery and a posteriori error estimates. Part 2: Error estimates and adaptivity, Internat. J. Numer. Methods Engrg., 1992, 33(7), 1365–1382